

# Gas Sensors Based on Titanium Oxides (Review)

Simonas Ramanavicius <sup>1,2</sup> , Arunas Jagminas <sup>1</sup> and Arunas Ramanavicius <sup>2,\*</sup> 

<sup>1</sup> Department of Electrochemical Material Science, Center for Physical Sciences and Technology (FTMC), Sauletekio Avenue 3, LT-10257 Vilnius, Lithuania; simonas.ramanavicius@ftmc.lt (S.R.); arunas.jagminas@ftmc.lt (A.J.)

<sup>2</sup> Department of Physical Chemistry, Faculty of Chemistry and Geosciences, Institute of Chemistry, Vilnius University, Naugarduko 24, LT-03225 Vilnius, Lithuania

\* Correspondence: arunas.ramanavicius@chf.vu.lt; Tel.: +370-60032332

**Abstract:** Nanostructured titanium compounds have recently been applied in the design of gas sensors. Among titanium compounds, titanium oxides (TiO<sub>2</sub>) are the most frequently used in gas sensing devices. Therefore, in this review, we are paying significant attention to the variety of allotropic modifications of titanium oxides, which include anatase, rutile, brookite. Very recently, the applicability of non-stoichiometric titanium oxide (TiO<sub>2-x</sub>)-based layers for the design of gas sensors was demonstrated. For this reason, in this review, we are addressing some research related to the formation of non-stoichiometric titanium oxide (TiO<sub>2-x</sub>) and Magnéli phase (Ti<sub>n</sub>O<sub>2n-1</sub>)-based layers suitable for sensor design. The most promising titanium compounds and hetero- and nano-structures based on these compounds are discussed. It is also outlined that during the past decade, many new strategies for the synthesis of TiO<sub>2</sub> and conducting polymer-based composite materials were developed, which have found some specific application areas. Therefore, in this review, we are highlighting how specific formation methods, which can be used for the formation of TiO<sub>2</sub> and conducting polymer composites, can be applied to tune composite characteristics that are leading towards advanced applications in these specific technological fields. The possibility to tune the sensitivity and selectivity of titanium compound-based sensing layers is addressed. In this review, some other recent reviews related to the development of sensors based on titanium oxides are overviewed. Some designs of titanium-based nanomaterials used for the development of sensors are outlined.

**Keywords:** titanium dioxide (TiO<sub>2</sub>); non-stoichiometric titanium oxide (TiO<sub>n</sub> or TiO<sub>2-x</sub>); magnéli phases (Ti<sub>n</sub>O<sub>2n-1</sub>); gas and volatile organic compounds (VOCs) sensors; nanostructures; MXenes; anatase; rutile; brookite



**Citation:** Ramanavicius, S.; Jagminas, A.; Ramanavicius, A. Gas Sensors Based on Titanium Oxides (Review). *Coatings* **2022**, *12*, 699. <https://doi.org/10.3390/coatings12050699>

Academic Editor: María Dolores Fernández Ramos

Received: 9 November 2021

Accepted: 16 May 2022

Published: 19 May 2022

**Publisher's Note:** MDPI stays neutral with regard to jurisdictional claims in published maps and institutional affiliations.



**Copyright:** © 2022 by the authors. Licensee MDPI, Basel, Switzerland. This article is an open access article distributed under the terms and conditions of the Creative Commons Attribution (CC BY) license (<https://creativecommons.org/licenses/by/4.0/>).

## 1. Introduction

Sensors for the determination of gasses and volatile organic compounds (VOCs) (gas-sensors) find applications in many different areas. Most of these gas sensors are based on semiconducting layers, which change their electrical resistance in the presence of gases and VOCs [1–7]. These semiconducting layers are mostly based on semiconductors such as WO<sub>3</sub>, MoS<sub>2</sub>, ZnO, SnO<sub>2</sub>, and TiO<sub>2</sub> TiO<sub>n</sub> [2–8], while Al<sub>2</sub>O<sub>3</sub> and SiO<sub>2</sub> are the most common dielectric substrates used for the formation of gas sensors. Some new titanium-based compounds, such as MXenes [9], and non-stoichiometric titanium oxides (TiO<sub>n</sub>) [1,2,10,11] have also been recently used in the design of gas sensors. The stoichiometric TiO<sub>2</sub> semiconductor of n-type, which appears in three major phases (rutile, anatase, and brookite) can be rather easily converted between these phases by thermal procedures, which paves the way to tune analytical characteristics of gas sensors [11]. These phases are sensitive and could be used for the detection of oxygen alone [12–14] or in heterostructures with ZrO<sub>2</sub> to improve sensing characteristics [15–17]. Besides stoichiometric TiO<sub>2</sub> forms, very recently, a non-stoichiometric (TiO<sub>n</sub>) that is sometimes indicated as TiO<sub>2-x</sub> has also been applied in

sensor design [1]. Titanium oxide structures based on specific Magnéli phases ( $\text{Ti}_n\text{O}_{2n-1}$ ) are very promising [10]. Many gas sensors are very sensitive, but mostly they are not very selective and consume a lot of electrical energy, which is required for the powering of the heater that is essential for the efficient operation of most gas sensors. In order to reduce the lastly mentioned disadvantage, the 'self-heating' strategy was developed, which enables the exploitation of the sensing layer as a heater of the analytical system [1,2,18]. Recently, some scientists have attempted to advance the selectivity of gas-sensors by the design of specific morphology of semiconducting structures [19,20], application of core-shell semiconducting nano-composites [21–23] and/or quantum dots [24,25]. Various aspects of titanium-based material are overviewed in recent reviews, addressing the properties, synthesis and modifications of  $\text{TiO}_2$ -based nanostructures [10,11,26]; application of titanium-based nanomaterials for energetics and environmental purposes [27]; the design of photo-catalysts [28]; the applicability of titanium oxides [1,2] and MXenes [9] in sensor design.

In this article, we are overviewing mainly the advances in the development of gas and volatile organic compounds (VOCs) sensors based on titanium-based oxides.

## 2. Structural Features and Physicochemical Properties of Stoichiometric and Non-Stoichiometric Titanium Oxides

$\text{TiO}_2$  belongs to n-type semiconducting materials [29,30]. Many  $\text{TiO}_2$ -based heterostructures are used in the design of sensors [11,31–34] and biosensors [35,36]. However, all the most popular forms of titanium oxides are characterized by specific bandgaps, which are as follows: (i) anatase by 3.02 eV (ii) rutile by 3.23 eV; (iii) brookite by 2.96 eV [37]. The annealing procedure is mostly used for the conversion of one titanium oxide phase into another one. Besides stoichiometric titanium oxide, plenty of non-stoichiometric forms were identified, among them very attractive conducting/semiconducting characteristics and gas-sensing properties [1]. They have Magnéli phases, which are described by  $\text{Ti}_n\text{O}_{2n-1}$  stoichiometry, where  $n = 4, \dots, 10$ . Their Magnéli phase neighbor is titanium pentoxide ( $\text{Ti}_3\text{O}_5$ ), where  $n = 3$  with a stoichiometry of  $\text{Ti}_n\text{O}_{2n-1}$ , which appears in a variety of different forms (that are indicated as  $\alpha$ -,  $\beta$ -,  $\gamma$ -,  $\delta$ -, and  $\lambda$ -) [38–42]. Stoichiometry of titanium pentoxide corresponds to that of the Magnéli phases ( $\text{Ti}_n\text{O}_{2n-1}$ ). Titanium pentoxide forms monoclinic crystals with the following lattice constants:  $a = 9.9701 \text{ \AA}$ ,  $b = 5.0747 \text{ \AA}$ ,  $c = 7.1810 \text{ \AA}$ ,  $\beta = 109.865^\circ$ . Moreover, titanium pentoxide, as well as some other Magnéli phases (e.g.,  $\text{Ti}_4\text{O}_7$ ), exhibit superconductivity when cooled down below 7 K temperature [43].

The most significant difference between titanium pentoxide and the Magnéli phases is determined by their different crystal structures. Magnéli phases contains shear planes based on  $\text{TiO}_2$ (rutile) [44,45], while in titanium pentoxide, such planes are absent [1,43]. A temperature of 400 °C is optimal for the appearance of  $\text{TiO}_2$ (anatase) intergrowths within  $\text{Ti}_3\text{O}_5$  crystals based on  $\text{TiO}_2$ -x/ $\text{TiO}_2$ -based heterostructures [46,47]. The incorporation of intergrowths based on  $\text{TiO}_2$ (anatase) in the structure of titanium pentoxide ( $\text{Ti}_3\text{O}_5$ ) improves their conductivity (Figure 1) and some photoluminescence-related characteristics [1]. It should be noted that such non-stoichiometric titanium oxides can be spontaneously oxidized for this reason and significant attention should be paid to the stabilization of these structures during their usage in the development of gas sensors. It should be noted that at different oxidation states, titanium oxides have different crystal structures [48], which starts from rutile for  $\text{TiO}_2$  and anatase for  $\text{Ti}_{10}\text{O}_{19}$  and then it turns into the triclinic structure for many stoichiometries, ranging from  $\text{Ti}_9\text{O}_{17}$  until  $\text{Ti}_4\text{O}_7$ , monoclinic for  $\gamma\text{Ti}_3\text{O}_5$ , tetragonal for  $\text{Ti}_2\text{O}_3$  and hexagonal for  $\text{TiO}$ ,  $\text{Ti}_2\text{O}$  and metallic titanium.

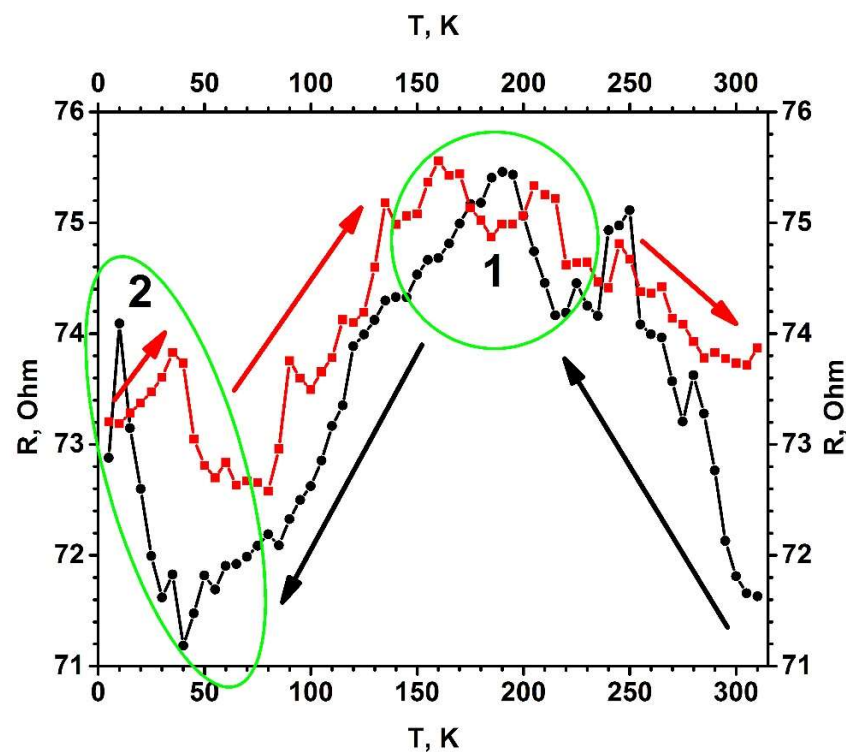


**Figure 1.** Temperature dependence of electrical resistance ( $R(T)$ ) for the  $\text{TiO}_{2-x}/\text{TiO}_2(400\text{ °C})$ -based hetero-structure. Temperature was changed in two ways (indicated by black and red arrows): (i) black circles shows points measured by cooling down, (ii) red squares shows points by increasing temperature. Measurements were performed in vacuum using helium cryostat. Figure adapted from [1].

The electrical conductivity of most non-stoichiometric titanium oxides is significantly higher than the conductivity of any allotropic form of stoichiometric titanium oxides ( $\text{TiO}_2$ ). The most significant increase in sensitivity is observed for titanium oxides with  $\text{Ti}_n\text{O}_{2n-1}$  stoichiometry, when index 'n' is in the range of 4–10 [49]. Some compounds with the above-mentioned stoichiometry form Magnéli phases, which are characterized by metallic conductivity and even by superconductivity [50,51].

Non-stoichiometric titanium oxide-based layers based on Magnéli phases have well conducting intergrowths based on  $\text{Ti}_n\text{O}_{2n-1}$  planar moieties that penetrate the  $\text{TiO}_2$ -based matrix [1,52]. Non-stoichiometric titanium oxides, such as  $\text{Ti}_2\text{O}_3$  and/or  $\text{Ti}_3\text{O}_5$ , which do not form real Magnéli phases anyway, are much better at conducting in comparison to stoichiometric  $\text{TiO}_2$  [1,43]. These n-type semiconducting titanium oxides have a high concentration of 'oxygen vacancies', which are responsible for the mobility of electrons through their structure [53] and baseline resistance [54]. It should be outlined that these 'oxygen vacancies' are also responsible for the sensitivity towards both oxidizing and reducing gases [1]. During the design of the sensing layer, initially formed stoichiometric titanium oxide-based layers can be chemically reduced into non-stoichiometric titanium oxide ( $\text{TiO}_{2-x}$ ) and/or Magnéli phases [2]. Magnéli phases are observed when the oxygen concentration in  $\text{TiO}_{2-x}$  structure is decreased and 'x' value is between 0.1 and 0.34 [1,55,56]. Non-stoichiometric titanium oxide structures containing Magnéli phases are chemically stable and rather well conducting. For these reasons, they are often applied in wastewater treatment and the design of batteries and fuel cells [57,58]; the same characteristics are required for gas sensors.

Non-stoichiometric titanium oxide-based structures can be developed using several approaches, namely plasma-treatment [59], laser irradiation-based modification [60], reduction by metallic zinc [61], bombardment by high-energy particles [62] and thermo-chemical approaches [63]. However, the formation of large  $\text{Ti}_3\text{O}_5$  monocrystals is rather challenging

because titanium oxides are polymorphic [43]. In some cases, stoichiometric titanium oxide can be easily turned into a non-stoichiometric one by suitable doping and/or reduction.

During the formation of  $\text{TiO}_{2-x}/\text{TiO}_2$ -based heterostructures, the ratio between stoichiometric titanium oxide and non-stoichiometric titanium oxide can be significantly increased by thermal treatment in reducing the gas atmosphere [64]. In several works, the transition between the insulator state and metallic state of  $\text{Ti}_3\text{O}_5$  ( $\beta$  and  $\lambda$  forms of  $\text{Ti}_3\text{O}_5$ , respectively) was performed by pulses of visible light [41] and by thermal treatment, which induced the conversion of  $\alpha$  form into  $\beta$  form at 450 K [38] and the conversion of  $\delta$  form into  $\gamma$  form at 240 K [39–42]. The phase transition of  $\text{Ti}_3\text{O}_5$  at 240–450 K is the most important for the adjustment of conductivity of this semiconducting material-based layers, e.g., the switching between metal and insulator states was observed at 350 K [43].

In some cases, non-stoichiometric titanium oxide can be formed by the partial oxidation of metallic titanium layers, which is followed by thermal treatment and annealing [1]. Sensors based on such structures, which are differently thermally treated and annealed, can be used in the formation of sensors with very different selectivity and sensitivity, which are suitable for the development of sensor arrays. Non-stoichiometric titanium oxide-based sensors, despite some significant advantages related to better catalytic activity and conductivity, have some disadvantages in comparison to those based on stoichiometric titanium oxides related to their insufficient stability at ambient conditions. In addition, it should be noted that the selectivity of these sensors is not superior.

### 3. Pristine Titanium Oxide-Based Gas Sensors and Their Sensing Mechanisms

Stoichiometric  $\text{TiO}_2$ -based gas sensors show high sensitivity to different gases. It should be noted that  $\text{TiO}_2$ -based gas sensors can rely on several different sensing mechanisms, which differ the most significantly for the determination of reducing gaseous compounds, such as  $\text{H}_2$ ,  $\text{H}_2\text{S}$ ,  $\text{NH}_3$ ,  $\text{CO}$ ,  $\text{CH}_3\text{OH}$ ,  $\text{C}_2\text{H}_5\text{OH}$ , etc. and for oxidizing gaseous compounds, such as  $\text{O}_2$ ,  $\text{NO}_2$ ,  $\text{CO}_2$  [28,63,65] (Table 1). The changes in electrical resistivity of the  $\text{TiO}_2$ -based layer are mostly used for the determination of analytical signals; therefore, the assessment of analytical signals generated by such sensors is rather simple. In some cases, measurement protocols were advanced by the determination of photoluminescence signals [1,2,8], which are generated by semiconducting  $\text{TiO}_2$  structures [66]. Some above-mentioned photocatalytic and photovoltaic properties can be improved by laser-based treatment [67]. However, the main disadvantage of  $\text{TiO}_2$ -based sensors is poor selectivity towards gaseous materials, which significantly complicates the application of these analytical devices. Therefore, in order to improve selectivity, various heterostructures containing  $\text{TiO}_2$  hybridized with many other semiconductors have been developed, e.g., our research group has developed a  $\text{TiO}_{2-x}/\text{TiO}_2$ -based self-heating heterostructure for the determination of  $\text{NH}_3$ ,  $\text{CH}_3\text{OH}$  and  $\text{C}_2\text{H}_5\text{OH}$  [1].

**Table 1.** Characteristics of titanium oxide-based sensors.

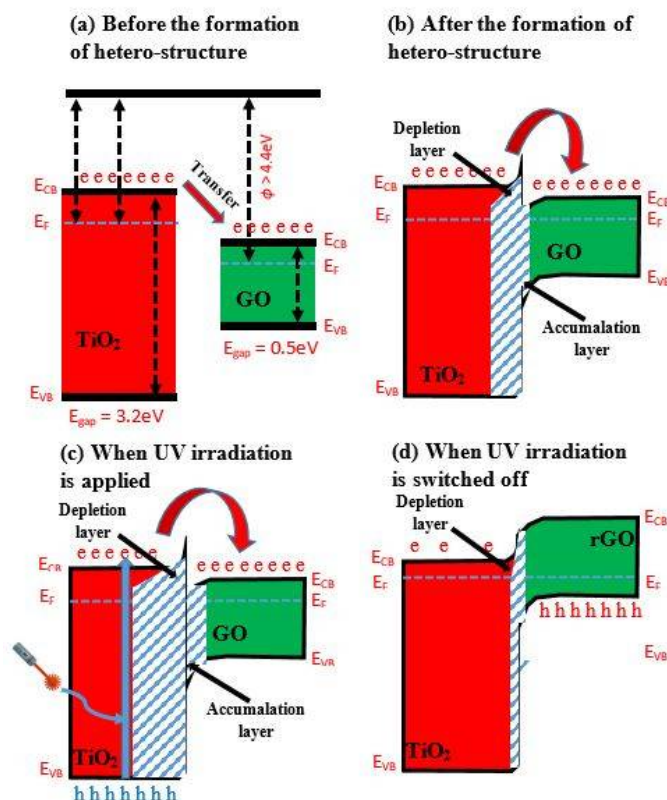
Sensing Material	Working Temperature	Gas Concentration	Response Value ( $R_a/R_g$ ) or ( $(\Delta R/R_g) \times 100\%$ )	Response Time	Recovery Time	Reference
$\text{TiO}_2$ (rutile), $\text{Ti}_8\text{O}_{15}$ and $\text{Ti}_9\text{O}_{17}$ mixture	210 °C	12.5–100 ppm ( $\text{NH}_3$ )	1–7%	2 min	8 min	[68]
$\text{TiO}_x$ -NiO	250–350 °C	100 ppm ( $\text{H}_2$ ) 100 ppm ( $\text{NO}_2$ ) 100 ppm ( $\text{NH}_3$ )	17 for $\text{H}_2$ (250 °C) 16 for $\text{NO}_2$ (250 °C) 4 for $\text{NH}_3$ (250 °C)	2 min	2, 3 min	[69]
$\beta$ - $\text{Ti}_3\text{O}_5$	150 °C	50 ppm ( $\text{H}_2$ )	11%	-	-	[70]

Table 1. Cont.

Sensing Material	Working Temperature	Gas Concentration	Response Value ( $R_a/R_g$ ) or ( $(\Delta R/R_g) \times 100\%$ )	Response Time	Recovery Time	Reference
Ti <sub>3</sub> O <sub>5</sub> -TiO <sub>2</sub> mixture	25–180 °C	105 ppm (H <sub>2</sub> O) 118 ppm (methanol) 53 ppm (ethanol) 18 ppm n-propanol 220 ppm (acetone)	0.5–18%	-	4–35 s	[1]
TiO <sub>2</sub> -Ti <sub>6</sub> O	150–450 °C	2000 ppm (H <sub>2</sub> ) 20 ppm (NO <sub>2</sub> ) 500 ppb (O <sub>3</sub> ) 1.6 ppm (acetone) 80 ppm (NO <sub>x</sub> )	2.9–348	8–21 s	20–32 s	[34]
Ti <sup>3+</sup> -TiO <sub>2</sub>	RT	100 ppm (CO)	39%	10 s	30 s	[71]
TiO <sub>2</sub>	150 °C	100 ppm (ethanol)	75.4%	155 s	779 s	[72]
TiO <sub>2</sub>	270 °C	500 ppm (acetone)	9.19	10 s	9 s	[73]
TiO <sub>2</sub>	350 °C	400 ppm (ethanol)	22.9	5 s	7 s	[74]
TiO <sub>2</sub>	RT	200 ppm (NH <sub>3</sub> )	64	28 s	24 s	[75]
α-Fe <sub>2</sub> O <sub>3</sub> -TiO <sub>2</sub>	325 °C	100 ppm (ethanol)	4	46 s	16 s	[76]

It was also reported that TiO<sub>2</sub> combined with La<sub>0.8</sub>Sr<sub>0.2</sub>Co<sub>0.5</sub>Ni<sub>0.5</sub>O<sub>3</sub> perovskite was applied for the determination of CO [77], TiO<sub>2</sub>/V<sub>2</sub>O<sub>5</sub>-based heterostructure for ozone [78], TiO<sub>2</sub>/SnO<sub>2</sub>-based heterostructure for NO<sub>2</sub> and CO [79,80]; TiO<sub>2</sub>/graphene (TiO<sub>2</sub>/GO)-based heterostructure for toluene determination at 298 K [81]. The action of TiO<sub>2</sub>/GO-based heterostructures based on the formed n-n hetero-junction is enhanced by UV irradiation [82] and is addressed in the band diagram presented in Figure 2a,b. The bandgap of the hetero-junction in the TiO<sub>2</sub>/GO-based heterostructure is 4.7 eV [83] which is higher than that of 4.4 eV and is usually observed for GO-based structures [84]; the formed hetero-structure has both accumulation and depletion layers [85] (Figure 2b). In this structure, a Schottky barrier is formed; therefore, the depletion layer in TiO<sub>2</sub> is thicker, and the number of electrons in the GO interface increases. The interaction of the adsorbed gases with the oxidized functional groups of GO induces variation in the resistance of the TiO<sub>2</sub>/GO-based heterostructure, which forms a sensing layer. In this heterostructure, TiO<sub>2</sub> is contributing by increasing the number of active sites suitable for the adsorption of gas molecules [86,87]. In some particular cases, activation energy can be lowered by adsorbed gas molecules, which increases the catalytic activity of the TiO<sub>2</sub> layer [88]. This property increases the sensitivity towards some reducing gases, such as ammonia, etc.; however, the active sites of GO are very sensitive towards moisture that increases electrical resistance, due to the interaction of water molecules with oxygen-based (carboxyl, carbonyl and hydroxyl) functional groups [89]. UV irradiation enables to solve this disadvantage by the increase in the depletion layer in TiO<sub>2</sub> and enhancement of the accumulation layer in GO (Figure 2c). Due to this reason, the electrons are shifted towards GO and reduced carboxyl, carbonyl and hydroxyl groups, which become unsuitable for the adsorption of water molecules [90]. This reduced GO establishes a p-n junction with TiO<sub>2</sub>, which at the interface is characterized

by decreased junction width (Figure 2d). UV irradiation of  $\text{TiO}_2$  induces the ‘injection’ of electrons into GO and in such a way that electron–hole pair recombination is prevented [91]. The surface concentration of adsorbed oxygen molecules decreases, which also reduces water sorption to this heterostructure [92]. The number of carboxyl, carbonyl and hydroxyl groups in GO structure can be partly restored by the UV irradiation-induced action of  $\text{TiO}_2$  [82].



**Figure 2.** Band diagram of  $\text{TiO}_2/\text{GO}$  hetero-structure (a) before the formation of hetero-structure, (b) after the formation of hetero-structure, (c) when UV irradiation is applied, and (d) when UV irradiation is switched off. (‘e’ is an electron; ‘h’ is a hole).

The heterostructure based on  $\text{TiO}_2/\text{SnO}_2$  is also very interesting because the depletion of energetic layers in the molecular orbitals of  $\text{TiO}_2$  electrons is induced when  $\text{TiO}_2$  is connected to  $\text{SnO}_2$  [79]. It should be noted that nanoparticle-based structures are preferable for the development of gas sensors [23] because the radius of nanoparticles based on some semiconducting materials that are used in the design of gas-sensors are in the same range as the Exciton Bohr radius; for this reason, such particles are very suitable for the design of gas sensors [25].

$\text{SnO}_2$  has great charge-carrier mobility, which is the most important factor for gas sensors based on resistivity measurements [80,93].  $\text{SnO}_2$ -based gas-sensing layers are cheap and stable at ambient conditions [94] however, it should be taken into account that sensors based on stoichiometric  $\text{TiO}_2$  and  $\text{SnO}_2$  operate at a rather high temperature, which exceeds several hundred degrees [25]. However, such sensors consume a lot of energy for the heating of the sensing layer; therefore, due to energy saving related issues, sensing layers capable to operate at low temperatures are under very special interest, e.g., sensing layers based on  $\text{Au}/\text{SnO}_2$  core-shell structures can operate in the temperature interval of 25–80 °C [95]. Our investigations of non-stoichiometric titanium oxide-based sensors shows that these sensors can operate even at room temperature [1,2]. It is expected that heterostructures based on  $\text{SnO}_2/\text{TiO}_2$  can be applied in low temperature gas sensors; therefore, some nanostructures were designed, which are as follows:  $\text{TiO}_2$  nanobelts

covered by SnO<sub>2</sub> [96], TiO<sub>2</sub>/SnO<sub>2</sub>-based core-shell nanofibers [97], SnO<sub>2</sub> layers doped by TiO<sub>2</sub> [98], structures based on SnO<sub>2</sub>/TiO<sub>2</sub> laminates [99], SnO<sub>2</sub> nanoparticles wrapped within TiO<sub>2</sub>-based nanofibers [79], SnO<sub>2</sub>-based quantum dots formed on a surface of TiO<sub>2</sub> layer were reported to be sensitive towards NO<sub>2</sub> and CO [100]. Atomic layer deposition (ALD) was used to deposit thin TiO<sub>2</sub> layers and it was demonstrated that tuning of the selectivity can be performed by the adjustment of TiO<sub>2</sub> layer thickness [101].

Significant energy consumptions for the heating of the sensing layer reduce the applicability of most gas sensors. Therefore, there is a demand for gas-sensing structures that can operate at low temperatures [102]. The miniaturization of sensing elements is another suitable strategy to reduce energy consumption. Low-temperature sensors based on titanium oxide-based layers were reported for O<sub>2</sub> [99], ozone [78], formaldehyde [103,104], CO [77], ethanol [96,98,105], C<sub>7</sub>H<sub>8</sub> [81], H<sub>2</sub> [106,107] and other gases [108].

The 'self-heating' of the sensing layer can be achieved when it has rather low resistance and part of electrical energy, which passes through this layer and is converted into thermal energy [1,2]. However, stoichiometric titanium oxide-based layers are characterised by a high band gap; therefore, the conductivity of these layers is not sufficient for 'self-heating' because rather high voltages are required to achieve some effect. On the contrary, this operation mode is very suitable for non-stoichiometric titanium oxide-based sensors, because these layers are good at conducting at low temperatures and in the temperature interval of 72–180 °C, these layers reach very good sensitivity towards some gases [1,2]. The semiconducting properties and chemical activity of titanium oxide enable sufficient catalytic and photocatalytic activities under UV irradiation to turn into a 'water splitting' ability [67,109], which eventually can be exploited for sensing purposes. It should be noted that at room temperature (298 K), sensing layers are sensitive to humidity. Therefore, analytical signals generated by adsorbed water molecules interfere with an analytical signal generated by target gases.

#### 4. The Action of Sensing Layers Based on TiO<sub>2</sub> Heterostructures and Assessment of Analytical Signals by Titanium Oxide-Based Sensors

The action of TiO<sub>2</sub>-based heterostructures relies on many parallel processes, where the most important are the adsorption of gas molecules to the surface of the sensing layer and the simultaneous desorption of gas, which was initially adsorbed to the same layer. Both adsorption and desorption events and/or the establishment of new chemical bonds between sensing TiO<sub>2</sub> layer and adsorbed gas molecules electrostatically affect the upper layer of the semiconducting TiO<sub>2</sub> layer and due to the depletion and/or enrichment of this layer by charge carriers, the conductivity of this layer changes correspondingly. The typical analytical signal determined by the adsorption and desorption of analyte gas is represented in Figure 3.

Several different types of electrical conductivity are observed in the TiO<sub>2</sub>-layers based on nano- or micro-particles, which are as follows: (i) intrinsic charge transfer through TiO<sub>2</sub>-particles and (ii) limitations of charge transfer through the boundaries between different particles. For this reason, the volume-concentration of these boundaries and the size/shape of particles are critical in the development of such sensors [110,111] (Figure 4). The semiconducting characteristics of TiO<sub>2</sub>-based structures, such as Debye length/radius, also strongly influence charge transfer in TiO<sub>2</sub>-based sensors. It should be noted that due to numerous thermal phase transitions during the annealing-based development of non-stoichiometric titanium oxide-based sensing structures, they are formed very porous and contain many different nanostructures and phases that significantly enhance the surface/volume ratio. Therefore, such structures are very efficient at absorbing gases, which leads to enhanced sensitivity of non-stoichiometric titanium oxide-based sensors. In order to achieve great sensitivity and selectivity, the discussed properties of non-stoichiometric titanium oxide-based sensing layers should be well tailored during the design of gas sensors [63,112–116].

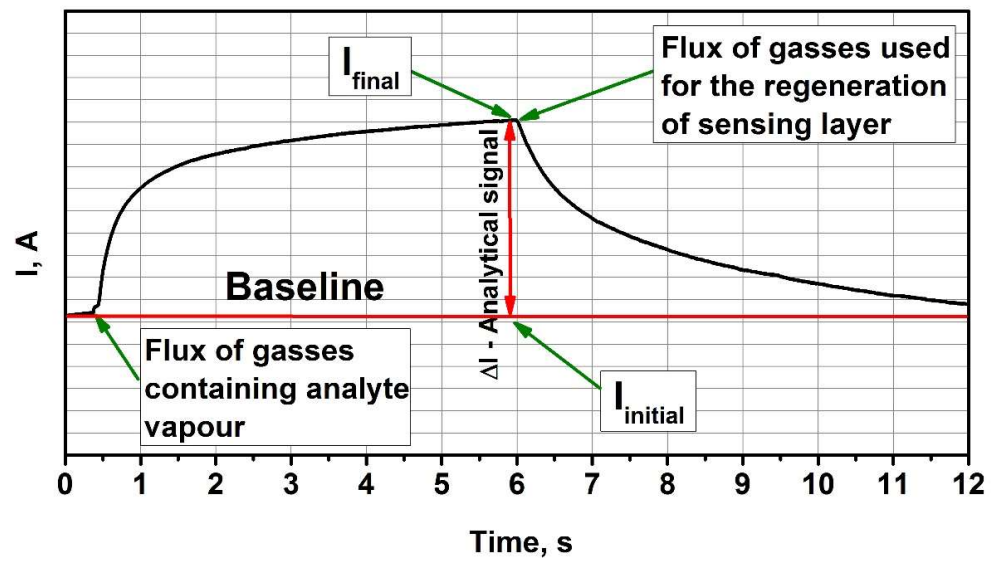


**Figure 3.** Representation of typical analytical signal for amperometric gas sensors. It should be noted that the duration of signal development and the regeneration of sensors highly depends on sensing material and sensing gases [1].

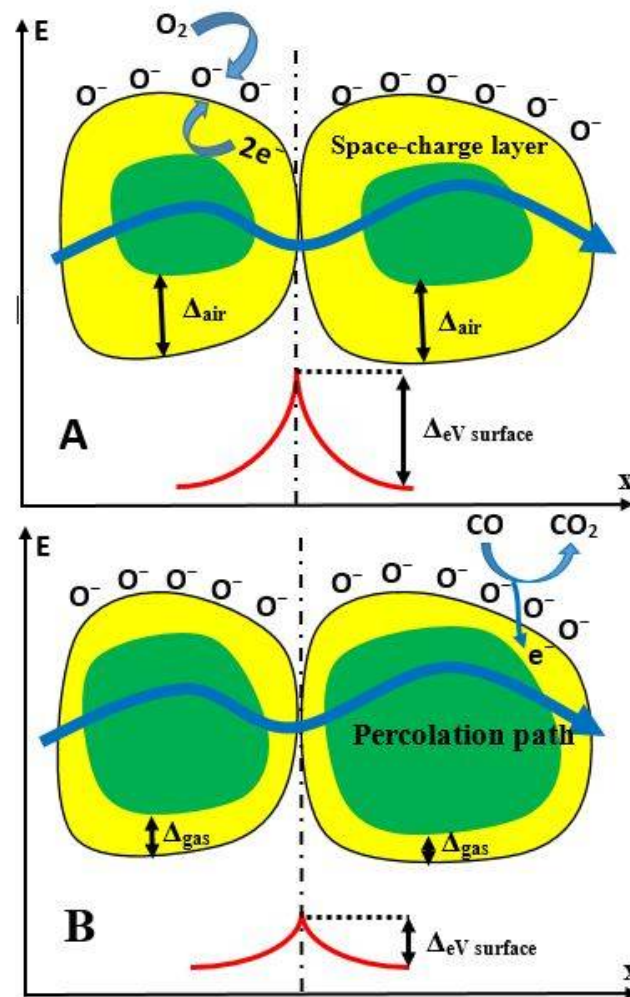


**Figure 4.** Representation of conductivity mechanism of semiconductor particle-based structure during the determination of CO gas. (A) Structure before the interaction with CO, (B) structure during the interaction with CO. Figure adapted from [2].

It should be noted that the adsorption of gas molecules with the surface of TiO<sub>2</sub>-based layer is a very complex process, which at a high extent is determined by Van der Waals and/or electrostatic interactions and/or the forming of new chemical bonds. Molecules of the gas that are present in the measurement cell before the introduction of analyte-gas containing aliquot are critically important for the establishment of the particular mechanism of sensing, because they are preabsorbing on the semiconducting structure and, in such a way, are responsible for the initial conductivity of the sensing layer. During the measurement, analyte gas containing aliquot appears in sensor-cell molecules of preadsorbed gas, which are replaced by analyte gas molecules (and/or by other gas molecules, which are part of aliquot). During both stages, adsorbed gas molecules are electrostatically interacting with the adsorption sites. It should be noted that in TiO<sub>2</sub>, defects of the crystal structure are acting as the most efficient adsorption sites. The adsorption ability of gas molecules very often depends on the ability to accept and/or to donate electrons to active sites that can be additionally involved in photoluminescence-based light emission [35]. Hence, donor/acceptor interactions change the electrical conductivity and the efficiency of photoluminescence of TiO<sub>2</sub>-based structures that can be used for the assessment of analyte concentration. However, stoichiometric titanium oxide-based structures are characterized by high resistance, which does not significantly vary in the presence of low concentrations of gaseous materials; therefore, the dynamic range of sensors based on stoichiometric titanium oxide is not high. Conducting polymers, especially polyaniline (PANI), are well suitable for the enhancement of the sensitivity of semiconducting metal oxides towards gases [117–119] and volatile compounds [120].

In order to increase sensitivity, various heterostructures containing TiO<sub>2</sub> are modified by other semiconducting materials, e.g., by conjugated polymers polyaniline (TiO<sub>2</sub>/PANI) and polypyrrole (TiO<sub>2</sub>/Ppy), which can be involved in the modification and design of titanium oxide-based sensing structures. The formation of the n/p-junction at TiO<sub>2</sub>/(conducting polymer) interphase is the most important factor for the enhancement of sensor sensitivity [121]. TiO<sub>2</sub>/Ppy-based sensing structures for the determination of NH<sub>3</sub> [122,123] propane/butane [124] and TiO<sub>2</sub>/PANI-based sensing structures for the detection of NH<sub>3</sub> [123,125–127] were developed. In order to improve sensitivity and selectivity, titanium oxide-based semiconducting structures can be modified by some metal oxides, carbides and other materials [1,2,9,113,114,128–131].

During the development of titanium oxide-based sensors, a very important issue is the elaboration of a suitable analytical signal registration protocol. The registration can be based on many physical approaches, including the measurement of photoluminescence response and electrical signals. Electrical signals can be determined from measurements performed in potentiostatic, galvanostatic and various potentiodynamic modes. If necessary, these modes can be combined with a 'self-heating' based approach. The determination of electrical conductivity measurements is most frequently used in gas sensors based on semiconducting structures [1,4,5,7,11,20,22–25,33,34,65,98,104,107,112,122,125,131,132]. At room temperature, stoichiometric titanium oxide-based sensing layers have a rather low conductivity of  $\sim 10^{-10}$  S/m; for this reason, up to 200–400 °C elevated temperature is applied in order to reach optimal electrical conductivity and sensing conditions. However, elevated temperatures increase the consumption of electrical energy required for the operation of the sensor.

## 5. TiO<sub>2</sub> and Conducting Polymer-Based Composites for Gas and VOC Sensors

The combination of metal oxide-based structures with conducting polymers led to the ability to tune precisely some properties of formed composite material in order to adjust it for specific applications [120]. Therefore, during the past decade, a lot of new strategies for the synthesis of different morphology TiO<sub>2</sub> (Figure 5) and their composites with conducting polymers were developed.

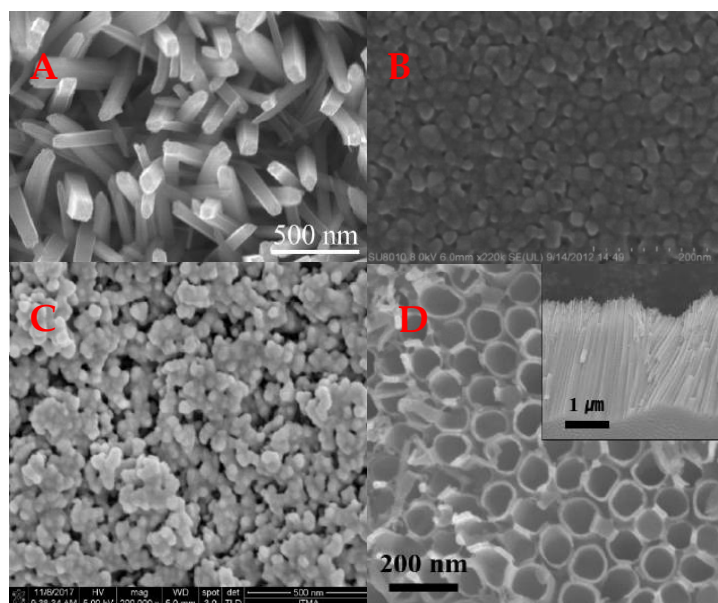


**Figure 5.** Different morphology TiO<sub>2</sub> structures used in design of a gas sensors. (A) Nanorods [133], (B) thin film [134], (C) nanoparticles [135], (D) nanotubes [136].

Chemical formation is one of the easiest and the most popular methods for the formation of TiO<sub>2</sub>-PANI composites. Usually, for chemical formation, acidic solutions (mostly HCl [137–139] or H<sub>2</sub>SO<sub>4</sub> [140,141]) are used together with reaction initiator (NH<sub>4</sub>)<sub>2</sub>S<sub>2</sub>O<sub>8</sub> [137–140,142]. Procedure protocols in most cases are similar and involve a few steps, which are as follows: (i) aniline and acid solution in distilled water together with TiO<sub>2</sub> is prepared in one beaker, (ii) in a second beaker, the polymerization initiator is dissolved in an acidic solution and (iii) both solutions are mixed, cooled to a near 0 °C temperature and stored for some time [137,138,143]. A visible sign of aniline polymerization reaction is a change of solution color into light blue, revealing the starting of PANI formation through an oxidation reaction. Finally, the reaction solution color becomes green, which indicates the successful formation of the PANI composite [139]. While varying in the parameters of reagent concentrations, it is possible that polymeric composite thickness, surface morphology and conductivity can be controlled by polymerization time and temperature depending on technological demand. It is important to mention that during the oxidation process, conductivity mainly depends on anions and their concentration used in the acid solution during the PANI polymerization reaction [137–140,143–145]. While wet chemical synthesis methods are the easiest to perform, electrochemical polymerization is one of the common methods, which provides relatively good control of the process in comparison to chemical formation. In this method, it is possible to use various modes for electrochemical PANI deposition on top of titanium dioxide substrate; however, the most popular modes are cyclic voltammetry (CV) [146–150] and chronoamperometry (CA) [146,150]. For CA depositions, a WE electrode potential in between 0.85–0.9 V vs. Ag/AgCl [146], while in CV mode, a potential in between –0.6–1.3 V vs. Ag/AgCl [146–149,151] and an acidic electrolyte with dissolved aniline are usually used [150,152].

Particularly, most researchers report that the modification of TiO<sub>2</sub>-based structures by conducting the polymer polyaniline (PANI) can increase their sensitivity towards some gases and/or VOC's [153,154]. An especially high number of researchers report that the modification of TiO<sub>2</sub>-based structures by PANI increases the sensitivity of designed sensors towards ammonia (NH<sub>3</sub>) [125,126,143,155–162]. The action mechanism of the sensing layer is rather simple; the conductivity sensing layer usually increases while oxygen, which is acting as an oxidizing agent, is physico-sorbed on TiO<sub>2</sub>/PANI and decreases when NH<sub>3</sub>, which is acting as a reducing agent, replaces the adsorbed oxygen [155]. Although all common PANI forms (including leucoemeraldine and pernigraniline) [163–165] can be used for

the modification of TiO<sub>2</sub>-based sensing layers, the most applicable seems to be an emeraldine form of PANI [154,157,159]. In addition to the most common TiO<sub>2</sub>-forms (anatase and rutile), recently a new trend is based on the application of various nonstoichiometric titanium suboxides, which are modified with conducting polymers including PANI [162,165], polypyrrole (Ppy) [123,124,166], polythiophene (PTH) [65], etc. Modifications by PANI are especially effective because PANI increases the sensitivity of titanium oxides towards NH<sub>3</sub> [125,126,143,155–162], H<sub>2</sub> [163,167], LPG [168,169] [170], CO<sub>2</sub> [169], trimethylamine (TMA) [160], H<sub>2</sub>S [160], benzene [138], toluene [169], cyclohexane [169], CO [165] and ethanol [164]. Analytical signals in most (titanium oxide)/PANI-based sensors are registered by the measurement of sensing layer resistance. However, there are some reports on the application of quartz crystal microbalances (QCM) in (titanium oxide)/PANI-based sensor design. Such TiO<sub>2</sub>-PANI composite-based QCM sensors were used for the detection of trimethylamine [170], hydrazine [148] and NH<sub>3</sub> [157].

## 6. Conclusions and Future Trends

A number of stoichiometric titanium oxide-based structures were applied in the design of gas sensors. However, these sensors still face selectivity-related problems, which can be solved by the doping of titanium oxide-based layers by dopants or the formation of hetero-structures based on a combination with some other semiconducting compounds and the adjustment of sensor-operation temperature. Among many others, sensors based on composite materials that are based on titanium oxide modified with conducting polymers are very promising, e.g., PANI. In recent investigations, it was shown that TiO<sub>2</sub>/TiO<sub>2-x</sub>-based heterostructures can be successfully applied in the design of gas sensors; it was demonstrated that the sensing properties of these sensors can be easily adjusted by changing the TiO<sub>2</sub>/TiO<sub>2-x</sub>-ratio heterostructures. Moreover, TiO<sub>2</sub>/TiO<sub>2-x</sub>-based heterostructures are good conductors; therefore, they can act in 'self-heating' mode and can reach temperatures that are suitable for the determination of some gaseous compounds. It is expected that TiO<sub>2</sub>/TiO<sub>2-x</sub>-based heterostructures will be more frequently applied in the design of gas sensors, but the main challenge in this research direction is still related to the control of stoichiometry and morphology of the TiO<sub>2</sub>/TiO<sub>2-x</sub>-based structure, which is very critical for the sensitivity and selectivity of the designed gas sensors.

**Author Contributions:** S.R. performed literature research, analysis, and drafted the paper. A.J. performed literature research, analysis, and drafted the paper. A.R. initiated and supervised the work and provided insights. All authors have read and agreed to the published version of the manuscript.

**Funding:** EU Horizon 2020 research and innovation programme H2020-MSCA-RISE under grant agreement № 778157 CanBioSe.

**Institutional Review Board Statement:** Not applicable.

**Informed Consent Statement:** Not applicable.

**Data Availability Statement:** Not applicable.

**Conflicts of Interest:** The authors declare no conflict of interest.

## References

1. Ramanavicius, S.; Tereshchenko, A.; Karpicz, R.; Ratautaite, V.; Bubniene, U.; Maneikis, A.; Jagminas, A.; Ramanavicius, A. TiO<sub>2-x</sub>/TiO<sub>2</sub>-Structure Based 'Self-Heated' Sensor for the Determination of Some Reducing Gases. *Sensors* **2020**, *20*, 74. [[CrossRef](#)] [[PubMed](#)]
2. Ramanavicius, S.; Ramanavicius, A. Insights in the Application of Stoichiometric and Non-Stoichiometric Titanium Oxides for the Design of Sensors for the Determination of Gases and VOCs (TiO<sub>2-x</sub> and TinO<sub>2n-1</sub> vs. TiO<sub>2</sub>). *Sensors* **2020**, *20*, 6833. [[CrossRef](#)] [[PubMed](#)]
3. Ramanavicius, S.; Petruleviciene, M.; Juodkazyte, J.; Griguceviciene, A.; Ramanavicius, A. Selectivity of Tungsten Oxide Synthesized by Sol-Gel Method Towards Some Volatile Organic Compounds and Gaseous Materials in a Broad Range of Temperatures. *Materials* **2020**, *13*, 523. [[CrossRef](#)] [[PubMed](#)]

4. Mirzaei, A.; Kim, S.S.; Kim, H.W. Resistance-Based H<sub>2</sub>S Gas Sensors Using Metal Oxide Nanostructures: A Review of Recent Advances. *J. Hazard. Mater.* **2018**, *357*, 314–331. [[CrossRef](#)] [[PubMed](#)]
5. Mirzaei, A.; Leonardi, S.G.; Neri, G. Detection of Hazardous Volatile Organic Compounds (VOCs) by Metal Oxide Nanostructures-Based Gas Sensors: A Review. *Ceram. Int.* **2016**, *42*, 15119–15141. [[CrossRef](#)]
6. Mirzaei, A.; Kim, J.H.; Kim, H.W.; Kim, S.S. How Shell Thickness Can Affect the Gas Sensing Properties of Nanostructured Materials: Survey of Literature. *Sens. Actuators B Chem.* **2018**, *258*, 270–294. [[CrossRef](#)]
7. Mirzaei, A.; Kim, J.-H.; Kim, H.W.; Kim, S.S. Resistive-Based Gas Sensors for Detection of Benzene, Toluene and Xylene (BTX) Gases: A Review. *J. Mater. Chem. C* **2018**, *6*, 4342–4370. [[CrossRef](#)]
8. Petrulėvičienė, M.; Juodkazytė, J.; Parvin, M.; Tereshchenko, A.; Ramanavicius, S.; Karpicz, R.; Samukaite-Bubniene, U.; Ramanavicius, A. Tuning the Photo-Luminescence Properties of WO<sub>3</sub> Layers by the Adjustment of Layer Formation Conditions. *Materials* **2020**, *13*, 2814. [[CrossRef](#)]
9. Ramanavicius, S.; Ramanavicius, A. Progress and Insights in the Application of MXenes as New 2D Nano-Materials Suitable for Biosensors and Biofuel Cell Design. *Int. J. Mol. Sci.* **2020**, *21*, 9224. [[CrossRef](#)]
10. Wang, Y.; Wu, T.; Zhou, Y.; Meng, C.; Zhu, W.; Liu, L. TiO<sub>2</sub>-Based Nanoheterostructures for Promoting Gas Sensitivity Performance: Designs, Developments, and Prospects. *Sensors* **2017**, *17*, 1971. [[CrossRef](#)]
11. Bai, J.; Zhou, B. Titanium Dioxide Nanomaterials for Sensor Applications. *Chem. Rev.* **2014**, *114*, 10131–10176. [[CrossRef](#)] [[PubMed](#)]
12. Mokrushin, A.S.; Gorban, Y.M.; Simonenko, N.P.; Simonenko, T.L.; Simonenko, E.P.; Sevastyanov, V.G.; Kuznetsov, N.T. Synthesis and Gas-Sensitive Chemoresistive Properties of TiO<sub>2</sub>-Cu Nanocomposite. *Russ. J. Inorg. Chem.* **2021**, *66*, 594–602. [[CrossRef](#)]
13. Mokrushin, A.S.; Simonenko, E.P.; Simonenko, N.P.; Akkuleva, K.T.; Antipov, V.V.; Zaharova, N.V.; Malygin, A.A.; Bukunov, K.A.; Sevastyanov, V.G.; Kuznetsov, N.T. Oxygen Detection Using Nanostructured TiO<sub>2</sub> Thin Films Obtained by the Molecular Layering Method. *Appl. Surf. Sci.* **2019**, *463*, 197–202. [[CrossRef](#)]
14. Sevastyanov, V.G.; Simonenko, E.P.; Simonenko, N.P.; Mokrushin, A.S.; Nikolaev, V.A.; Kuznetsov, N.T. Sol-Gel Made Titanium Dioxide Nanostructured Thin Films as Gas-Sensing Materials for the Detection of Oxygen. *Mendeleev Commun.* **2018**, *28*, 164–166. [[CrossRef](#)]
15. Mokrushin, A.S.; Simonenko, E.P.; Simonenko, N.P.; Bukunov, K.A.; Gorobtsov, P.Y.; Sevastyanov, V.G.; Kuznetsov, N.T. Gas-Sensing Properties of Nanostructured TiO<sub>2</sub>-xZrO<sub>2</sub> Thin Films Obtained by the Sol-Gel Method. *J. Sol-Gel Sci. Technol.* **2019**, *92*, 415–426. [[CrossRef](#)]
16. Simonenko, E.P.; Simonenko, N.P.; Kopitsa, G.P.; Mokrushin, A.S.; Khamova, T.V.; Sizova, S.V.; Khaddazh, M.; Tsvigun, N.V.; Pipich, V.; Gorshkova, Y.E.; et al. A Sol-Gel Synthesis and Gas-Sensing Properties of Finely Dispersed ZrTiO<sub>4</sub>. *Mater. Chem. Phys.* **2019**, *225*, 347–357. [[CrossRef](#)]
17. Simonenko, E.P.; Mokrushin, A.S.; Simonenko, N.P.; Voronov, V.A.; Kim, V.P.; Tkachev, S.V.; Gubin, S.P.; Sevastyanov, V.G.; Kuznetsov, N.T. Ink-Jet Printing of a TiO<sub>2</sub>-10%ZrO<sub>2</sub> Thin Film for Oxygen Detection Using a Solution of Metal Alkoxoacetylacetonates. *Thin Solid Film.* **2019**, *670*, 46–53. [[CrossRef](#)]
18. Prades, J.D.; Jimenez-Diaz, R.; Hernandez-Ramirez, F.; Barth, S.; Cirera, A.; Romano-Rodriguez, A.; Mathur, S.; Morante, J.R. Ultralow Power Consumption Gas Sensors Based on Self-Heated Individual Nanowires. *Appl. Phys. Lett.* **2008**, *93*, 123110. [[CrossRef](#)]
19. Smulko, J.M.; Trawka, M.; Granqvist, C.G.; Ionescu, R.; Annanouch, F.; Llobet, E.; Kish, L.B. New Approaches for Improving Selectivity and Sensitivity of Resistive Gas Sensors: A Review. *Sens. Rev.* **2015**, *35*, 340–347. [[CrossRef](#)]
20. Simon, I.; Bãrsan, N.; Bauer, M.; Weimar, U. Micromachined Metal Oxide Gas Sensors: Opportunities to Improve Sensor Performance. *Sens. Actuators B Chem.* **2001**, *73*, 1–26. [[CrossRef](#)]
21. Karnati, P.; Akbar, S.; Morris, P.A. Conduction Mechanisms in One Dimensional Core-Shell Nanostructures for Gas Sensing: A Review. *Sens. Actuators B Chem.* **2019**, *295*, 127–143. [[CrossRef](#)]
22. Kim, J.H.; Mirzaei, A.; Kim, H.W.; Kim, S.S. Low Power-Consumption CO Gas Sensors Based on Au-Functionalized SnO<sub>2</sub>-ZnO Core-Shell Nanowires. *Sens. Actuators B Chem.* **2018**, *267*, 597–607. [[CrossRef](#)]
23. Mirzaei, A.; Janghorban, K.; Hashemi, B.; Bonavita, A.; Bonyani, M.; Leonardi, S.G.; Neri, G. Synthesis, Characterization and Gas Sensing Properties of Ag@α-Fe<sub>2</sub>O<sub>3</sub> Core-Shell Nanocomposites. *Nanomaterials* **2015**, *5*, 737–749. [[CrossRef](#)] [[PubMed](#)]
24. Deng, J.; Fu, Q.; Luo, W.; Tong, X.; Xiong, J.; Hu, Y.; Zheng, Z. Enhanced H<sub>2</sub>S Gas Sensing Properties of Undoped ZnO Nanocrystalline Films from QDs by Low-Temperature Processing. *Sens. Actuators B Chem.* **2016**, *224*, 153–158. [[CrossRef](#)]
25. Mosadegh Sedghi, S.; Mortazavi, Y.; Khodadadi, A. Low Temperature CO and CH<sub>4</sub> Dual Selective Gas Sensor Using SnO<sub>2</sub> Quantum Dots Prepared by Sonochemical Method. *Sens. Actuators B Chem.* **2010**, *145*, 7–12. [[CrossRef](#)]
26. Chen, X.; Mao, S.S. Titanium Dioxide Nanomaterials: Synthesis, Properties, Modifications, and Applications. *Chem. Rev.* **2007**, *107*, 2891–2959. [[CrossRef](#)]
27. Zhang, Y.; Jiang, Z.; Huang, J.; Lim, L.Y.; Li, W.; Deng, J.; Gong, D.; Tang, Y.; Lai, Y.; Chen, Z. Titanate and Titania Nanostructured Materials for Environmental and Energy Applications: A Review. *RSC Adv.* **2015**, *5*, 79479–79510. [[CrossRef](#)]
28. Linsebigler, A.L.; Lu, G.; Yates, J.T. Photocatalysis on TiO<sub>2</sub> Surfaces: Principles, Mechanisms, and Selected Results. *Chem. Rev.* **1995**, *95*, 735–758. [[CrossRef](#)]
29. Soni, P.; Murty, V.V.S.; Kushwaha, K.K. The Effect of Ni<sup>2+</sup> Ions on Energy Band Gap of TiO<sub>2</sub> Nanoparticles for Solar Cell Applications. *J. Nanosci. Nanoeng. Appl* **2018**, *8*, 69–74.

30. Yamazoe, N.; Sakai, G.; Shimanoe, K. Oxide Semiconductor Gas Sensors. *Catal. Surv. Asia* **2003**, *7*, 63–75. [[CrossRef](#)]
31. Wang, G.; Wang, J.; An, Y.; Wang, C. Anodization Fabrication of 3D TiO<sub>2</sub> Photonic Crystals and Their Application for Chemical Sensors. *Superlattices Microstruct.* **2016**, *100*, 290–295. [[CrossRef](#)]
32. Si, H.; Pan, N.; Zhang, X.; Liao, J.; Romyantseva, M.N.; Gaskov, A.M.; Lin, S. A Real-Time on-Line Photoelectrochemical Sensor toward Chemical Oxygen Demand Determination Based on Field-Effect Transistor Using an Extended Gate with 3D TiO<sub>2</sub> Nanotube Arrays. *Sens. Actuators B Chem.* **2019**, *289*, 106–113. [[CrossRef](#)]
33. Qiu, J.; Zhang, S.; Zhao, H. Recent Applications of TiO<sub>2</sub> Nanomaterials in Chemical Sensing in Aqueous Media. *Sens. Actuators B: Chem.* **2011**, *160*, 875–890. [[CrossRef](#)]
34. Maziarz, W.; Kusior, A.; Trenczek-Zajac, A. Nanostructured TiO<sub>2</sub>-Based Gas Sensors with Enhanced Sensitivity to Reducing Gases. *Beilstein J. Nanotechnol.* **2016**, *7*, 1718–1726. [[CrossRef](#)] [[PubMed](#)]
35. Tereshchenko, A.; Smyntyna, V.; Ramanavicius, A. Interaction Mechanism between TiO<sub>2</sub> Nanostructures and Bovine Leukemia Virus Proteins in Photoluminescence-Based Immunosensors. *RSC Adv.* **2018**, *8*, 37740–37748. [[CrossRef](#)] [[PubMed](#)]
36. Tereshchenko, A.; Viter, R.; Konup, I.; Ivanitsa, V.; Geveliuk, S.; Ishkov, Y.; Smyntyna, V. TiO<sub>2</sub> Optical Sensor for Amino Acid Detection. In Proceedings of the Biophotonics—Riga 2013, Riga, Latvia, 26–31 August 2013; Spigulis, J., Kuzmina, I., Eds.; SPIE: Washington, DC, USA, 2013; Volume 9032, pp. 186–190.
37. Wunderlich, W.; Oekermann, T.; Miao, L.; Hue, N.T.; Tanemura, S.; Tanemura, M. ELECTRONIC PROPERTIES OF NANOPOROUS TiO<sub>2</sub>- AND ZnO THIN FILMS- COMPARISON OF SIMULATIONS AND EXPERIMENTS. *J. Ceram. Process. Res.* **2004**, *5*, 343–354.
38. Åsbrink, S.; Magnéli, A. Crystal Structure Studies on Trititanium Pentoxide, Ti<sub>3</sub>O<sub>5</sub>. *Acta Crystallogr.* **1959**, *12*, 575–581. [[CrossRef](#)]
39. Hong, S.-H.; Åsbrink, S. The Structure of  $\gamma$ -Ti<sub>3</sub>O<sub>5</sub> at 297 K. *Acta Crystallogr. Sect. B* **1982**, *38*, 2570–2576. [[CrossRef](#)]
40. Onoda, M. Phase Transitions of Ti<sub>3</sub>O<sub>5</sub>. *J. Solid State Chem.* **1998**, *136*, 67–73. [[CrossRef](#)]
41. Ohkoshi, S.; Tsunobuchi, Y.; Matsuda, T.; Hashimoto, K.; Namai, A.; Hakoe, F.; Tokoro, H. Synthesis of a Metal Oxide with a Room-Temperature Photoreversible Phase Transition. *Nat. Chem.* **2010**, *2*, 539–545. [[CrossRef](#)]
42. Tanaka, K.; Nasu, T.; Miyamoto, Y.; Ozaki, N.; Tanaka, S.; Nagata, T.; Hakoe, F.; Yoshikiyo, M.; Nakagawa, K.; Umetsu, Y.; et al. Structural Phase Transition between  $\gamma$ -Ti<sub>3</sub>O<sub>5</sub> and  $\delta$ -Ti<sub>3</sub>O<sub>5</sub> by Breaking of a One-Dimensionally Conducting Pathway. *Cryst. Growth Des.* **2015**, *15*, 653–657. [[CrossRef](#)]
43. Yoshimatsu, K.; Sakata, O.; Ohtomo, A. Superconductivity in Ti<sub>4</sub>O<sub>7</sub> and  $\gamma$ -Ti<sub>3</sub>O<sub>5</sub> Films. *Sci. Rep.* **2017**, *7*, 12544. [[CrossRef](#)] [[PubMed](#)]
44. Marezio, M.; McWhan, D.B.; Dernier, P.D.; Remeika, J.P. Structural Aspects of the Metal-Insulator Transitions in Ti<sub>4</sub>O<sub>7</sub>. *J. Solid State Chem.* **1973**, *6*, 213–221. [[CrossRef](#)]
45. Lakkis, S.; Schlenker, C.; Chakraverty, B.K.; Buder, R.; Marezio, M. Metal-Insulator Transitions in Ti<sub>4</sub>O<sub>7</sub> Single Crystals: Crystal Characterization, Specific Heat, and Electron Paramagnetic Resonance. *Phys. Rev. B* **1976**, *14*, 1429–1440. [[CrossRef](#)]
46. D'Angelo, A.M.; Webster, N.A.S. Evidence of Anatase Intergrowths Formed during Slow Cooling of Reduced Ilmenite. *J. Appl. Crystallogr.* **2018**, *51*, 185–192. [[CrossRef](#)]
47. Grey, I.E.; Cranswick, L.M.D.; Li, C.; White, T.J.; Bursill, L.A. New M<sub>3</sub>O<sub>5</sub>-Anatase Intergrowth Structures Formed during Low-Temperature Oxidation of Anosovite. *J. Solid State Chem.* **2000**, *150*, 128–138. [[CrossRef](#)]
48. Jayashree, S.; Ashokkumar, M. Switchable Intrinsic Defect Chemistry of Titania for Catalytic Applications. *Catalysts* **2018**, *8*, 601. [[CrossRef](#)]
49. Andersson, S.; Magnéli, A. Diskrete Titanoxydphasen Im Zusammensetzungsbereich TiO<sub>1,75</sub>-TiO<sub>1,90</sub>. *Naturwissenschaften* **1956**, *43*, 495–496. [[CrossRef](#)]
50. Liborio, L.; Mallia, G.; Harrison, N. Electronic Structure of the Ti<sub>4</sub>O<sub>7</sub> Magnéli Phase. *Phys. Rev. B* **2009**, *79*, 245133. [[CrossRef](#)]
51. Liborio, L.; Harrison, N. Thermodynamics of Oxygen Defective Magnéli Phases in Rutile: A First-Principles Study. *Phys. Rev. B* **2008**, *77*, 104104. [[CrossRef](#)]
52. Adamaki, V.; Clemens, F.; Ragulis, P.; Pennock, S.R.; Taylor, J.; Bowen, C.R. Manufacturing and Characterization of Magnéli Phase Conductive Fibres. *J. Mater. Chem. A* **2014**, *2*, 8328–8333. [[CrossRef](#)]
53. Zhu, Q.; Peng, Y.; Lin, L.; Fan, C.-M.; Gao, G.-Q.; Wang, R.-X.; Xu, A.-W. Stable Blue TiO<sub>2-x</sub> Nanoparticles for Efficient Visible Light Photocatalysts. *J. Mater. Chem. A* **2014**, *2*, 4429–4437. [[CrossRef](#)]
54. Al-Hashem, M.; Akbar, S.; Morris, P. Role of Oxygen Vacancies in Nanostructured Metal-Oxide Gas Sensors: A Review. *Sens. Actuators B Chem.* **2019**, *301*, 126845. [[CrossRef](#)]
55. Seebauer, E.G.; Kratzer, M.C. Charged Point Defects in Semiconductors. *Mater. Sci. Eng. R Rep.* **2006**, *55*, 57–149. [[CrossRef](#)]
56. Harada, S.; Tanaka, K.; Inui, H. Thermoelectric Properties and Crystallographic Shear Structures in Titanium Oxides of the Magnéli Phases Bandgap Engineering of Magnéli Phase Ti<sub>n</sub>O<sub>2n-1</sub>: Electron-Hole Self-Compensation. *J. Appl. Phys.* **2010**, *108*, 83703. [[CrossRef](#)]
57. Smith, J.R.; Walsh, F.C.; Clarke, R.L. Electrodes Based on Magnéli Phase Titanium Oxides: The Properties and Applications of Ebonex<sup>®</sup> Materials. *J. Appl. Electrochem.* **1998**, *28*, 1021–1033. [[CrossRef](#)]
58. Walsh, F.C.; Wills, R.G.A. The Continuing Development of Magnéli Phase Titanium Sub-Oxides and Ebonex<sup>®</sup> Electrodes. *Electrochim. Acta* **2010**, *55*, 6342–6351. [[CrossRef](#)]
59. Nakamura, I.; Negishi, N.; Kutsuna, S.; Ihara, T.; Sugihara, S.; Takeuchi, K. Role of Oxygen Vacancy in the Plasma-Treated TiO<sub>2</sub> Photocatalyst with Visible Light Activity for NO Removal. *J. Mol. Catal. A Chem.* **2000**, *161*, 205–212. [[CrossRef](#)]

60. le Mercier, T.; Mariot, J.M.; Parent, P.; Fontaine, M.F.; Hague, C.F.; Quarton, M. Formation of  $Ti^{3+}$  Ions at the Surface of Laser-Irradiated Rutile. *Appl. Surf. Sci.* **1995**, *86*, 382–386. [[CrossRef](#)]
61. Zheng, Z.; Huang, B.; Meng, X.; Wang, J.; Wang, S.; Lou, Z.; Wang, Z.; Qin, X.; Zhang, X.; Dai, Y. Metallic Zinc-Assisted Synthesis of  $Ti^{3+}$  Self-Doped  $TiO_2$  with Tunable Phase Composition and Visible-Light Photocatalytic Activity. *Chem. Commun.* **2013**, *49*, 868–870. [[CrossRef](#)]
62. Hashimoto, S.; Tanaka, A. Alteration of Ti 2p XPS Spectrum for Titanium Oxide by Low-Energy Ar Ion Bombardment. *Surf. Interface Anal.* **2002**, *34*, 262–265. [[CrossRef](#)]
63. Wang, Y.; Du, G.; Liu, H.; Liu, D.; Qin, S.; Wang, N.; Hu, C.; Tao, X.; Jiao, J.; Wang, J.; et al. Nanostructured Sheets of Ti—O Nanobelts for Gas Sensing and Antibacterial Applications. *Adv. Funct. Mater.* **2008**, *18*, 1131–1137. [[CrossRef](#)]
64. Hayfield, P.C.S. *Development of a New Material: Monolithic  $Ti_4O_7$  Ebonex Ceramic*; Royal Society of Chemistry: London, UK, 2007; ISBN 184755069X.
65. Kimura, M.; Sakai, R.; Sato, S.; Fukawa, T.; Ikehara, T.; Maeda, R.; Mihara, T. Sensing of Vaporous Organic Compounds by  $TiO_2$  Porous Films Covered with Polythiophene Layers. *Adv. Funct. Mater.* **2012**, *22*, 469–476. [[CrossRef](#)]
66. Viter, R.; Tereshchenko, A.; Smyntyna, V.; Ogorodniichuk, J.; Starodub, N.; Yakimova, R.; Khranovskyy, V.; Ramanavicius, A. Toward Development of Optical Biosensors Based on Photoluminescence of  $TiO_2$  Nanoparticles for the Detection of Salmonella. *Sens. Actuators B Chem.* **2017**, *252*, 95–102. [[CrossRef](#)]
67. Haryński, L.; Grochowska, K.; Karczewski, J.; Ryl, J.; Siuzdak, K. Scalable Route toward Superior Photoresponse of UV-Laser-Treated  $TiO_2$  Nanotubes. *ACS Appl. Mater. Interfaces* **2020**, *12*, 3225–3235. [[CrossRef](#)]
68. Gardon, M.; Monereo, O.; Dosta, S.; Vescio, G.; Cirera, A.; Guilemany, J.M. New Procedures for Building-up the Active Layer of Gas Sensors on Flexible Polymers. *Surf. Coat. Technol.* **2013**, *235*, 848–852. [[CrossRef](#)]
69. Imawan, C.; Solzbacher, F.; Steffes, H.; Obermeier, E.  $TiO_x$ -Modified NiO Thin Films for  $H_2$  Gas Sensors: Effects of  $TiO_x$ -Overlayer Sputtering Parameters. *Sens. Actuators B Chem.* **2000**, *68*, 184–188. [[CrossRef](#)]
70. Li, X.; Liu, Y.; Ma, S.; Ye, J.; Zhang, X.; Wang, G.; Qiu, Y. The Synthesis and Gas Sensitivity of the  $\beta$ - $Ti_3O_5$  Powder: Experimental and DFT Study. *J. Alloys Compd.* **2015**, *649*, 939–948. [[CrossRef](#)]
71. Su, J.; Zou, X.-X.; Zou, Y.-C.; Li, G.-D.; Wang, P.-P.; Chen, J.-S. Porous Titania with Heavily Self-Doped  $Ti^{3+}$  for Specific Sensing of CO at Room Temperature. *Inorg. Chem.* **2013**, *52*, 5924–5930. [[CrossRef](#)]
72. Gakhar, T.; Hazra, A. Oxygen Vacancy Modulation of Titania Nanotubes by Cathodic Polarization and Chemical Reduction Routes for Efficient Detection of Volatile Organic Compounds. *Nanoscale* **2020**, *12*, 9082–9093. [[CrossRef](#)]
73. Navale, S.T.; Yang, Z.B.; Liu, C.; Cao, P.J.; Patil, V.B.; Ramgir, N.S.; Mane, R.S.; Stadler, F.J. Enhanced Acetone Sensing Properties of Titanium Dioxide Nanoparticles with a Sub-Ppm Detection Limit. *Sens. Actuators B Chem.* **2018**, *255*, 1701–1710. [[CrossRef](#)]
74. Gao, X.; Li, Y.; Zeng, W.; Zhang, C.; Wei, Y. Hydrothermal Synthesis of Agglomerating  $TiO_2$  Nanoflowers and Its Gas Sensing. *J. Mater. Sci. Mater. Electron.* **2017**, *28*, 18781–18786. [[CrossRef](#)]
75. Mintcheva, N.; Srinivasan, P.; Rayappan, J.B.B.; Kuchmizhak, A.A.; Gurbatov, S.; Kulinich, S.A. Room-Temperature Gas Sensing of Laser-Modified Anatase  $TiO_2$  Decorated with Au Nanoparticles. *Appl. Surf. Sci.* **2020**, *507*, 145169. [[CrossRef](#)]
76. Mei, H.; Zhou, S.; Lu, M.; Zhao, Y.; Cheng, L. Construction of Pine-Branch-like  $\alpha$ - $Fe_2O_3/TiO_2$  Hierarchical Heterostructure for Gas Sensing. *Ceram. Int.* **2020**, *46*, 18675–18682. [[CrossRef](#)]
77. Hsu, K.C.; Fang, T.H.; Hsiao, Y.J.; Wu, P.C. Response and Characteristics of  $TiO_2$ /Perovskite Heterojunctions for CO Gas Sensors. *J. Alloys Compd.* **2019**, *794*, 576–584. [[CrossRef](#)]
78. Avansi, W.; Catto, A.C.; da Silva, L.F.; Fiorido, T.; Bernardini, S.; Mastelaro, V.R.; Aguir, K.; Arenal, R. One-Dimensional  $V_2O_5/TiO_2$  Heterostructures for Chemiresistive Ozone Sensors. *ACS Appl. Nano Mater.* **2019**, *2*, 4756–4764. [[CrossRef](#)]
79. Chen, K.; Chen, S.; Pi, M.; Zhang, D.  $SnO_2$  Nanoparticles/ $TiO_2$  Nanofibers Heterostructures: In Situ Fabrication and Enhanced Gas Sensing Performance. *Solid-State Electron.* **2019**, *157*, 42–47. [[CrossRef](#)]
80. Yu, Q.; Zhu, J.; Xu, Z.; Huang, X. Facile Synthesis of  $\alpha$ - $Fe_2O_3@SnO_2$  Core-Shell Heterostructure Nanotubes for High Performance Gas Sensors. *Sens. Actuators B Chem.* **2015**, *213*, 27–34. [[CrossRef](#)]
81. Seekaew, Y.; Wisitsoraat, A.; Phokharatkul, D.; Wongchoosuk, C. Room Temperature Toluene Gas Sensor Based on  $TiO_2$  Nanoparticles Decorated 3D Graphene-Carbon Nanotube Nanostructures. *Sens. Actuators B Chem.* **2019**, *279*, 69–78. [[CrossRef](#)]
82. Lee, E.; Lee, D.; Yoon, J.; Yin, Y.; Lee, Y.N.; Uprety, S.; Yoon, Y.S.; Kim, D.-J. Enhanced Gas-Sensing Performance of GO/ $TiO_2$  Composite by Photocatalysis. *Sensors* **2018**, *18*, 3334. [[CrossRef](#)]
83. Stratakis, E.; Savva, K.; Konios, D.; Petridis, C.; Kymakis, E. Improving the Efficiency of Organic Photovoltaics by Tuning the Work Function of Graphene Oxide Hole Transporting Layers. *Nanoscale* **2014**, *6*, 6925–6931. [[CrossRef](#)] [[PubMed](#)]
84. Chen, C.; Cai, W.; Long, M.; Zhou, B.; Wu, Y.; Wu, D.; Feng, Y. Synthesis of Visible-Light Responsive Graphene Oxide/ $TiO_2$  Composites with p/n Heterojunction. *ACS Nano* **2010**, *4*, 6425–6432. [[CrossRef](#)] [[PubMed](#)]
85. Lightcap, I.V.; Kosel, T.H.; Kamat, P. Anchoring Semiconductor and Metal Nanoparticles on a Two-Dimensional Catalyst Mat. Storing and Shuttling Electrons with Reduced Graphene Oxide. *Nano Lett.* **2010**, *10*, 577–583. [[CrossRef](#)] [[PubMed](#)]
86. Ammu, S.; Dua, V.; Agnihotra, S.R.; Surwade, S.P.; Phulgirkar, A.; Patel, S.; Manohar, S.K. Flexible, All-Organic Chemiresistor for Detecting Chemically Aggressive Vapors. *J. Am. Chem. Soc.* **2012**, *134*, 4553–4556. [[CrossRef](#)] [[PubMed](#)]
87. Lam, K.C.; Huang, B.; Shi, S.-Q. Room-Temperature Methane Gas Sensing Properties Based on in Situ Reduced Graphene Oxide Incorporated with Tin Dioxide. *J. Mater. Chem. A* **2017**, *5*, 11131–11142. [[CrossRef](#)]

88. Ye, Z.; Tai, H.; Xie, T.; Yuan, Z.; Liu, C.; Jiang, Y. Room Temperature Formaldehyde Sensor with Enhanced Performance Based on Reduced Graphene Oxide/Titanium Dioxide. *Sens. Actuators B Chem.* **2016**, *223*, 149–156. [[CrossRef](#)]
89. Buchsteiner, A.; Lerf, A.; Pieper, J. Water Dynamics in Graphite Oxide Investigated with Neutron Scattering. *J. Phys. Chem. B* **2006**, *110*, 22328–22338. [[CrossRef](#)]
90. Phan, D.T.; Chung, G.S. Effects of Rapid Thermal Annealing on Humidity Sensor Based on Graphene Oxide Thin Films. *Sens. Actuators B Chem.* **2015**, *220*, 1050–1055. [[CrossRef](#)]
91. Wang, P.; Zhai, Y.; Wang, D.; Dong, S. Synthesis of Reduced Graphene Oxide-Anatase TiO<sub>2</sub> Nanocomposite and Its Improved Photo-Induced Charge Transfer Properties. *Nanoscale* **2011**, *3*, 1640–1645. [[CrossRef](#)]
92. Cui, S.; Wen, Z.; Huang, X.; Chang, J.; Chen, J. Stabilizing MoS<sub>2</sub> Nanosheets through SnO<sub>2</sub> Nanocrystal Decoration for High-Performance Gas Sensing in Air. *Small* **2015**, *11*, 2305–2313. [[CrossRef](#)]
93. Mirzaei, A.; Janghorban, K.; Hashemi, B.; Neri, G. Metal-Core@metal Oxide-Shell Nanomaterials for Gas-Sensing Applications: A Review. *J. Nanoparticle Res.* **2015**, *17*, 371. [[CrossRef](#)]
94. Rieu, M.; Camara, M.; Tournier, G.; Viricelle, J.P.; Pijolat, C.; de Rooij, N.F.; Briand, D. Fully Inkjet Printed SnO<sub>2</sub> Gas Sensor on Plastic Substrate. *Sens. Actuators B Chem.* **2016**, *236*, 1091–1097. [[CrossRef](#)]
95. Chung, F.C.; Wu, R.J.; Cheng, F.C. Fabrication of a Au@SnO<sub>2</sub> Core–Shell Structure for Gaseous Formaldehyde Sensing at Room Temperature. *Sens. Actuators B Chem.* **2014**, *190*, 1–7. [[CrossRef](#)]
96. Chen, G.; Ji, S.; Li, H.; Kang, X.; Chang, S.; Wang, Y.; Yu, G.; Lu, J.; Claverie, J.; Sang, Y.; et al. High-Energy Faceted SnO<sub>2</sub>-Coated TiO<sub>2</sub> Nanobelt Heterostructure for Near-Ambient Temperature-Responsive Ethanol Sensor. *ACS Appl. Mater. Interfaces* **2015**, *7*, 24950–24956. [[CrossRef](#)]
97. Li, F.; Gao, X.; Wang, R.; Zhang, T.; Lu, G. Study on TiO<sub>2</sub>-SnO<sub>2</sub> Core-Shell Heterostructure Nanofibers with Different Work Function and Its Application in Gas Sensor. *Sens. Actuators B Chem.* **2017**, *248*, 812–819. [[CrossRef](#)]
98. Zeng, W.; Liu, T.; Wang, Z. UV Light Activation of TiO<sub>2</sub> Doped SnO<sub>2</sub> Thick Film for Sensing Ethanol at Room Temperature. *Mater. Trans.* **2010**, *51*, 243–245. [[CrossRef](#)]
99. Lee, H.C.; Hwang, W.S. Substrate Effects on the Oxygen Gas Sensing Properties of SnO<sub>2</sub>/TiO<sub>2</sub> Thin Films. *Appl. Surf. Sci.* **2006**, *253*, 1889–1897. [[CrossRef](#)]
100. Lee, J.H.; Mirzaei, A.; Kim, J.H.; Kim, J.Y.; Nasriddinov, A.F.; Romyantseva, M.N.; Kim, H.W.; Kim, S.S. Gas-Sensing Behaviors of TiO<sub>2</sub>-Layer-Modified SnO<sub>2</sub> Quantum Dots in Self-Heating Mode and Effects of the TiO<sub>2</sub> Layer. *Sens. Actuators B Chem.* **2020**, *310*, 127870. [[CrossRef](#)]
101. Ng, S.; Prášek, J.; Zazpe, R.; Pytlíček, Z.; Spatz, Z.; Pereira, J.R.; Michalička, J.; Příkryl, J.; Krbal, M.; Sopha, H.; et al. Atomic Layer Deposition of SnO<sub>2</sub>-Coated Anodic One-Dimensional TiO<sub>2</sub> Nanotube Layers for Low Concentration NO<sub>2</sub> Sensing. *ACS Appl. Mater. Interfaces* **2020**, *12*, 33386–33396. [[CrossRef](#)]
102. Song, Z.; Wei, Z.; Wang, B.; Luo, Z.; Xu, S.; Zhang, W.; Yu, H.; Li, M.; Huang, Z.; Zang, J.; et al. Sensitive Room-Temperature H<sub>2</sub>S Gas Sensors Employing SnO<sub>2</sub> Quantum Wire/Reduced Graphene Oxide Nanocomposites. *Chem. Mater.* **2016**, *28*, 1205–1212. [[CrossRef](#)]
103. Nasriddinov, A.; Romyantseva, M.; Marikutsa, A.; Gaskov, A.; Lee, J.-H.; Kim, J.-H.; Kim, J.-Y.; Kim, S.S.; Kim, H.W. Sub-Ppm Formaldehyde Detection by n-n TiO<sub>2</sub>@SnO<sub>2</sub> Nanocomposites. *Sensors* **2019**, *19*, 3182. [[CrossRef](#)] [[PubMed](#)]
104. Li, X.; Li, X.; Wang, J.; Lin, S. Highly Sensitive and Selective Room-Temperature Formaldehyde Sensors Using Hollow TiO<sub>2</sub> Microspheres. *Sens. Actuators B Chem.* **2015**, *219*, 158–163. [[CrossRef](#)]
105. Righettoni, M.; Tricoli, A.; Pratsinis, S.E. Minimal Cross-Sensitivity to Humidity during Ethanol Detection by SnO<sub>2</sub>-TiO<sub>2</sub> Solid Solutions Related Content Toward Portable Breath Acetone Analysis for Diabetes Detection Minimal Cross-Sensitivity to Humidity during Ethanol Detection by SnO<sub>2</sub>-TiO<sub>2</sub> Solid Solutions. *Nanotechnology* **2009**, *20*, 10. [[CrossRef](#)]
106. Li, Z.; Yao, Z.J.; Haidry, A.A.; Plecenik, T.; Xie, L.J.; Sun, L.C.; Fatima, Q. Resistive-Type Hydrogen Gas Sensor Based on TiO<sub>2</sub>: A Review. *Int. J. Hydrogen Energy* **2018**, *43*, 21114–21132. [[CrossRef](#)]
107. Shaposhnik, D.; Pavelko, R.; Llobet, E.; Gispert-Guirado, F.; Vilanova, X. Hydrogen Sensors on the Basis of SnO<sub>2</sub>-TiO<sub>2</sub> Systems. *Sens. Actuators B: Chem.* **2012**, *174*, 527–534. [[CrossRef](#)]
108. Plecenik, T.; Moško, M.; Haidry, A.A.; Ďurina, P.; Truchlý, M.; Grančič, B.; Gregor, M.; Roch, T.; Satrapinskyy, L.; Mošková, A.; et al. Fast Highly-Sensitive Room-Temperature Semiconductor Gas Sensor Based on the Nanoscale Pt-TiO<sub>2</sub>-Pt Sandwich. *Sens. Actuators B Chem.* **2015**, *207*, 351–361. [[CrossRef](#)]
109. Lin, J.; Heo, Y.-U.; Nattestad, A.; Sun, Z.; Wang, L.; Kim, J.H.; Dou, S.X. 3D Hierarchical Rutile TiO<sub>2</sub> and Metal-Free Organic Sensitizer Producing Dye-Sensitized Solar Cells 8.6% Conversion Efficiency. *Sci. Rep.* **2014**, *4*, 5769. [[CrossRef](#)]
110. Wang, C.; Yin, L.; Zhang, L.; Xiang, D.; Gao, R. Metal Oxide Gas Sensors: Sensitivity and Influencing Factors. *Sensors* **2010**, *10*, 2088–2106. [[CrossRef](#)]
111. Franke, M.E.; Koplín, T.J.; Simon, U. Metal and Metal Oxide Nanoparticles in Chemiresistors: Does the Nanoscale Matter? *Small* **2006**, *2*, 36–50. [[CrossRef](#)]
112. Wang, C.; Yin, L.; Zhang, L.; Qi, Y.; Lun, N.; Liu, N. Large Scale Synthesis and Gas-Sensing Properties of Anatase TiO<sub>2</sub> Three-Dimensional Hierarchical Nanostructures. *Langmuir* **2010**, *26*, 12841–12848. [[CrossRef](#)]
113. Barreca, D.; Comini, E.; Ferrucci, A.P.; Gasparotto, A.; Maccato, C.; Maragno, C.; Sberveglieri, G.; Tondello, E. First Example of ZnO–TiO<sub>2</sub> Nanocomposites by Chemical Vapor Deposition: Structure, Morphology, Composition, and Gas Sensing Performances. *Chem. Mater.* **2007**, *19*, 5642–5649. [[CrossRef](#)]

114. Lü, R.; Zhou, W.; Shi, K.; Yang, Y.; Wang, L.; Pan, K.; Tian, C.; Ren, Z.; Fu, H. Alumina Decorated TiO<sub>2</sub> Nanotubes with Ordered Mesoporous Walls as High Sensitivity NO<sub>x</sub> Gas Sensors at Room Temperature. *Nanoscale* **2013**, *5*, 8569–8576. [[CrossRef](#)] [[PubMed](#)]
115. Li, Z.; Ding, D.; Liu, Q.; Ning, C.; Wang, X. Ni-Doped TiO<sub>2</sub> Nanotubes for Wide-Range Hydrogen Sensing. *Nanoscale Res. Lett.* **2014**, *9*, 118. [[CrossRef](#)] [[PubMed](#)]
116. Galstyan, V.; Comini, E.; Faglia, G.; Sberveglieri, G. TiO<sub>2</sub> Nanotubes: Recent Advances in Synthesis and Gas Sensing Properties. *Sensors* **2013**, *13*, 14813–14838. [[CrossRef](#)] [[PubMed](#)]
117. Ratautaite, V.; Bagdziunas, G.; Ramanavicius, A.; Ramanaviciene, A. An Application of Conducting Polymer Polypyrrole for the Design of Electrochromic PH and CO<sub>2</sub> Sensors. *J. Electrochem. Soc.* **2019**, *166*, B297–B303. [[CrossRef](#)]
118. Celiesiute, R.; Ramanaviciene, A.; Gicevicius, M.; Ramanavicius, A. Electrochromic Sensors Based on Conducting Polymers, Metal Oxides, and Coordination Complexes. *Crit. Rev. Anal. Chem.* **2019**, *49*, 195–208. [[CrossRef](#)]
119. Popov, A.; Brasiunas, B.; Mikoliunaite, L.; Bagdziunas, G.; Ramanavicius, A.; Ramanaviciene, A. Comparative Study of Polyaniline (PANI), Poly(3,4-Ethylenedioxythiophene) (PEDOT) and PANI-PEDOT Films Electrochemically Deposited on Transparent Indium Thin Oxide Based Electrodes. *Polym. (Guildf)* **2019**, *172*, 133–141. [[CrossRef](#)]
120. Turemis, M.; Zappi, D.; Giardi, M.T.; Basile, G.; Ramanaviciene, A.; Kapralovs, A.; Ramanavicius, A.; Viter, R. ZnO/Polyaniline Composite Based Photoluminescence Sensor for the Determination of Acetic Acid Vapor. *Talanta* **2020**, *211*, 120658. [[CrossRef](#)]
121. Miller, D.R.; Akbar, S.A.; Morris, P.A. Nanoscale Metal Oxide-Based Heterojunctions for Gas Sensing: A Review. *Sens. Actuators B Chem.* **2014**, *204*, 250–272. [[CrossRef](#)]
122. Wu, Y.; Xing, S.; Fu, J. Examining the Use of TiO<sub>2</sub> to Enhance the NH<sub>3</sub> Sensitivity of Polypyrrole Films. *J. Appl. Polym. Sci.* **2010**, *118*, 3351–3356. [[CrossRef](#)]
123. Tai, H.; Jiang, Y.; Xie, G.; Yu, J.; Zhao, M. International Journal of Environmental Analytical Chemistry Self-Assembly of TiO<sub>2</sub>/Polypyrrole Nanocomposite Ultrathin Films and Application for an NH<sub>3</sub> Gas Sensor. *Int. J. Environ. Anal. Chem.* **2007**, *87*, 539–551. [[CrossRef](#)]
124. Bulakhe, R.N.; Patil, S.V.; Deshmukh, P.R.; Shinde, N.M.; Lokhande, C.D. Fabrication and Performance of Polypyrrole (Ppy)/TiO<sub>2</sub> Heterojunction for Room Temperature Operated LPG Sensor. *Sens. Actuators B Chem.* **2013**, *181*, 417–423. [[CrossRef](#)]
125. Gong, J.; Li, Y.; Hu, Z.; Zhou, Z.; Deng, Y. Ultrasensitive NH<sub>3</sub> Gas Sensor from Polyaniline Nanograin Enchased TiO<sub>2</sub> Fibers. *J. Phys. Chem. C* **2010**, *114*, 9970–9974. [[CrossRef](#)]
126. Pawar, S.G.; Chougule, M.A.; Sen, S.; Patil, V.B. Development of Nanostructured Polyaniline–Titanium Dioxide Gas Sensors for Ammonia Recognition. *J. Appl. Polym. Sci.* **2012**, *125*, 1418–1424. [[CrossRef](#)]
127. Wang, Q.; Dong, X.; Pang, Z.; Du, Y.; Xia, X.; Wei, Q.; Huang, F. Ammonia Sensing Behaviors of TiO<sub>2</sub>-PANI/PA6 Composite Nanofibers. *Sensors* **2012**, *12*, 17046–17057. [[CrossRef](#)] [[PubMed](#)]
128. Du, P.; Song, L.; Xiong, J.; Li, N.; Xi, Z.; Wang, L.; Jin, D.; Guo, S.; Yuan, Y. Coaxial Electrospun TiO<sub>2</sub>/ZnO Core–Sheath Nanofibers Film: Novel Structure for Photoanode of Dye-Sensitized Solar Cells. *Electrochim. Acta* **2012**, *78*, 392–397. [[CrossRef](#)]
129. Ding, Y.; Wang, Y.; Zhang, L.; Zhang, H.; Li, C.M.; Lei, Y. Preparation of TiO<sub>2</sub>-Pt Hybrid Nanofibers and Their Application for Sensitive Hydrazine Detection. *Nanoscale* **2011**, *3*, 1149–1157. [[CrossRef](#)]
130. Li, Z.; Zhang, H.; Zheng, W.; Wang, W.; Huang, H.; Wang, C.; MacDiarmid, A.G.; Wei, Y. Highly Sensitive and Stable Humidity Nanosensors Based on LiCl Doped TiO<sub>2</sub> Electrospun Nanofibers. *J. Am. Chem. Soc.* **2008**, *130*, 5036–5037. [[CrossRef](#)]
131. Zeng, W.; Liu, T.; Wang, Z. Enhanced Gas Sensing Properties by SnO<sub>2</sub> Nanosphere Functionalized TiO<sub>2</sub> Nanobelts. *J. Mater. Chem.* **2012**, *22*, 3544–3548. [[CrossRef](#)]
132. Zakrzewska, K. Gas Sensing Mechanism of TiO<sub>2</sub>-Based Thin Films. *Vacuum* **2004**, *74*, 335–338. [[CrossRef](#)]
133. Liang, Y.-C.; Liu, Y.-C. Design of Nanoscaled Surface Morphology of TiO<sub>2</sub>-Ag<sub>2</sub>O Composite Nanorods through Sputtering Decoration Process and Their Low-Concentration NO<sub>2</sub> Gas-Sensing Behaviors. *Nanomaterials* **2019**, *9*, 1150. [[CrossRef](#)] [[PubMed](#)]
134. Wang, H.; Chen, L.; Wang, J.; Sun, Q.; Zhao, Y. A Micro Oxygen Sensor Based on a Nano Sol-Gel TiO<sub>2</sub> Thin Film. *Sensors* **2014**, *14*, 16423–16433. [[CrossRef](#)] [[PubMed](#)]
135. SA, M.C.; Hamidon, M.N.; Mamat, M.S.; Ertugrul, M.; Abdullah, N.H. A Hydrogen Gas Sensor Based on TiO<sub>2</sub> Nanoparticles on Alumina Substrate. *Sensors* **2018**, *18*, 2483. [[CrossRef](#)]
136. Park, S.; Kim, S.; Park, S.; Lee, W.I.; Lee, C. Effects of Functionalization of TiO<sub>2</sub> Nanotube Array Sensors with Pd Nanoparticles on Their Selectivity. *Sensors* **2014**, *14*, 15849–15860. [[CrossRef](#)] [[PubMed](#)]
137. Yavuz, A.G.; Gök, A. Preparation of TiO<sub>2</sub>/PANI Composites in the Presence of Surfactants and Investigation of Electrical Properties. *Synth. Met.* **2007**, *157*, 235–242. [[CrossRef](#)]
138. Oh, M.; Park, S.J.; Jung, Y.; Kim, S. Electrochemical Properties of Polyaniline Composite Electrodes Prepared by In-Situ Polymerization in Titanium Dioxide Dispersed Aqueous Solution. *Synth. Met.* **2012**, *162*, 695–701. [[CrossRef](#)]
139. Guo, N.; Liang, Y.; Lan, S.; Liu, L.; Zhang, J.; Ji, G.; Gan, S. Microscale Hierarchical Three-Dimensional Flowerlike TiO<sub>2</sub>/PANI Composite: Synthesis, Characterization, and Its Remarkable Photocatalytic Activity on Organic Dyes under UV-Light and Sunlight Irradiation. *J. Phys. Chem. C* **2014**, *118*, 18343–18355. [[CrossRef](#)]
140. Gottam, R.; Srinivasan, P. One-Step Oxidation of Aniline by Peroxotitanium Acid to Polyaniline–Titanium Dioxide: A Highly Stable Electrode for a Supercapacitor. *J. Appl. Polym. Sci.* **2015**, *132*. [[CrossRef](#)]
141. Radoičić, M.; Šaponjić, Z.; Nedeljković, J.; Ćirić-Marjanović, G.; Stejskal, J. Self-Assembled Polyaniline Nanotubes and Nanoribbons/Titanium Dioxide Nanocomposites. *Synth. Met.* **2010**, *160*, 1325–1334. [[CrossRef](#)]

142. Su, S.J.; Kuramoto, N. Processable Polyaniline–Titanium Dioxide Nanocomposites: Effect of Titanium Dioxide on the Conductivity. *Synth. Met.* **2000**, *114*, 147–153. [[CrossRef](#)]
143. Tai, H.; Jiang, Y.; Xie, G.; Yu, J.; Chen, X. Fabrication and Gas Sensitivity of Polyaniline–Titanium Dioxide Nanocomposite Thin Film. *Sens. Actuators B Chem.* **2007**, *125*, 644–650. [[CrossRef](#)]
144. Lee, I.S.; Lee, J.Y.; Sung, J.H.; Choi, H.J. Synthesis and Electrochemical Characteristics of Polyaniline–Titanium Dioxide Hybrid Suspension. *Synth. Met.* **2005**, *152*, 173–176. [[CrossRef](#)]
145. Kang, K.S. Effect of Excess Amount of Aniline for TiO<sub>2</sub> and Polyaniline Composite. *Synth. Met.* **2016**, *217*, 197–201. [[CrossRef](#)]
146. Maldonado-Larios, L.; Mayen-Mondragón, R.; Martínez-Orozco, R.D.; Páramo-García, U.; Gallardo-Rivas, N.V.; García-Alamilla, R. Electrochemically-Assisted Fabrication of Titanium-Dioxide/Polyaniline Nanocomposite Films for the Electroremediation of Congo Red in Aqueous Effluents. *Synth. Met.* **2020**, *268*, 116464. [[CrossRef](#)]
147. Ilieva, M.; Ivanov, S.; Tsakova, V. Electrochemical Synthesis and Characterization of TiO<sub>2</sub>-Polyaniline Composite Layers. *J. Appl. Electrochem.* **2008**, *38*, 63–69. [[CrossRef](#)]
148. Saeb, E.; Asadpour-Zeynali, K. Facile Synthesis of TiO<sub>2</sub>@PANI@Au Nanocomposite as an Electrochemical Sensor for Determination of Hydrazine. *Microchem. J.* **2021**, *160*, 105603. [[CrossRef](#)]
149. Cai, G.; Tu, J.; Zhou, D.; Zhang, J.; Xiong, Q.; Zhao, X.; Wang, X.; Gu, C. Multicolor Electrochromic Film Based on TiO<sub>2</sub>@Polyaniline Core/Shell Nanorod Array. *J. Phys. Chem. C* **2013**, *117*, 15967–15975. [[CrossRef](#)]
150. Gobal, F.; Faraji, M. Electrodeposited Polyaniline on Pd-Loaded TiO<sub>2</sub> Nanotubes as Active Material for Electrochemical Supercapacitor. *J. Electroanal. Chem.* **2013**, *691*, 51–56. [[CrossRef](#)]
151. Jagminas, A.; Balčiūnaitė, A.; Niaura, G.; Tamašauskaitė-Tamašiūnaitė, L. Electrochemical Synthesis and Characterisation of Polyaniline in TiO<sub>2</sub> Nanotubes. *Trans. IMF* **2012**, *90*, 311–315. [[CrossRef](#)]
152. Patil, B.H.; Jang, K.; Lee, S.; Kim, J.H.; Yoon, C.S.; Kim, J.; Kim, D.H.; Ahn, H. Periodically Ordered Inverse Opal TiO<sub>2</sub>/Polyaniline Core/Shell Design for Electrochemical Energy Storage Applications. *J. Alloys Compd.* **2017**, *694*, 111–118. [[CrossRef](#)]
153. Gao, L.; Yin, C.; Luo, Y.; Duan, G. Facile Synthesis of the Composites of Polyaniline and TiO<sub>2</sub> Nanoparticles Using Self-Assembly Method and Their Application in Gas Sensing. *Nanomaterials* **2019**, *9*, 493. [[CrossRef](#)]
154. Ma, X.; Wang, M.; Li, G.; Chen, H.; Bai, R. Preparation of Polyaniline–TiO<sub>2</sub> Composite Film with in Situ Polymerization Approach and Its Gas-Sensitivity at Room Temperature. *Mater. Chem. Phys.* **2006**, *98*, 241–247. [[CrossRef](#)]
155. Huyen, D.N.; Tung, N.T.; Thien, N.D.; Thanh, L.H. Effect of TiO<sub>2</sub> on the Gas Sensing Features of TiO<sub>2</sub>/PANi Nanocomposites. *Sensors* **2011**, *11*, 1924–1931. [[CrossRef](#)]
156. Tai, H.; Jiang, Y.; Xie, G.; Yu, J.; Chen, X.; Ying, Z. Influence of Polymerization Temperature on NH<sub>3</sub> Response of PANI/TiO<sub>2</sub> Thin Film Gas Sensor. *Sens. Actuators B Chem.* **2008**, *129*, 319–326. [[CrossRef](#)]
157. Bairi, V.G.; Bourdo, S.E.; Sacre, N.; Nair, D.; Berry, B.C.; Biris, A.S.; Viswanathan, T. Ammonia Gas Sensing Behavior of Tanninsulfonic Acid Doped Polyaniline–TiO<sub>2</sub> Composite. *Sensors* **2015**, *15*, 26415–26429. [[CrossRef](#)]
158. Pawar, S.G.; Chougule, M.A.; Patil, S.L.; Raut, B.T.; Godse, P.R.; Sen, S.; Patil, V.B. Room Temperature Ammonia Gas Sensor Based on Polyaniline–TiO<sub>2</sub> Nanocomposite. *IEEE Sens J* **2011**, *11*, 3417–3423. [[CrossRef](#)]
159. Seif, A.; Nikfarjam, A.; Hajghassem, H. UV Enhanced Ammonia Gas Sensing Properties of PANI/TiO<sub>2</sub> Core-Shell Nanofibers. *Sens. Actuators B Chem.* **2019**, *298*, 126906. [[CrossRef](#)]
160. Cui, S.; Wang, J.; Wang, X. Fabrication and Design of a Toxic Gas Sensor Based on Polyaniline/Titanium Dioxide Nanocomposite Film by Layer-by-Layer Self-Assembly. *RSC Adv.* **2015**, *5*, 58211–58219. [[CrossRef](#)]
161. Zhu, C.; Cheng, X.; Dong, X. Enhanced Sub-Ppm NH<sub>3</sub> Gas Sensing Performance of PANI/TiO<sub>2</sub> Nanocomposites at Room Temperature. *Front. Chem.* **2018**, *6*, 493. [[CrossRef](#)]
162. Li, Y.; Gong, J.; He, G.; Deng, Y. Fabrication of Polyaniline/Titanium Dioxide Composite Nanofibers for Gas Sensing Application. *Mater. Chem. Phys.* **2011**, *129*, 477–482. [[CrossRef](#)]
163. Nasirian, S.; Milani Moghaddam, H. Effect of Different Titania Phases on the Hydrogen Gas Sensing Features of Polyaniline/TiO<sub>2</sub> Nanocomposite. *Polymer (Guildf)* **2014**, *55*, 1866–1874. [[CrossRef](#)]
164. Gawri, I.; Ridhi, R.; Singh, K.P.; Tripathi, S.K. Chemically Synthesized TiO<sub>2</sub> and PANI/TiO<sub>2</sub> Thin Films for Ethanol Sensing Applications. *Mater. Res. Express* **2018**, *5*, 025303. [[CrossRef](#)]
165. Wang, Z.; Peng, X.; Huang, C.; Chen, X.; Dai, W.; Fu, X. CO Gas Sensitivity and Its Oxidation over TiO<sub>2</sub> Modified by PANI under UV Irradiation at Room Temperature. *Appl. Catal. B Environ.* **2017**, *219*, 379–390. [[CrossRef](#)]
166. Su, P.G.; Huang, L.N. Humidity Sensors Based on TiO<sub>2</sub> Nanoparticles/Polypyrrole Composite Thin Films. *Sens. Actuators B Chem.* **2007**, *123*, 501–507. [[CrossRef](#)]
167. Srivastava, S.; Kumar, S.; Singh, V.N.; Singh, M.; Vijay, Y.K. Synthesis and Characterization of TiO<sub>2</sub> Doped Polyaniline Composites for Hydrogen Gas Sensing. *Int. J. Hydrogen Energy* **2011**, *36*, 6343–6355. [[CrossRef](#)]
168. Dhawale, D.S.; Salunkhe, R.R.; Patil, U.M.; Gurav, K.V.; More, A.M.; Lokhande, C.D. Room Temperature Liquefied Petroleum Gas (LPG) Sensor Based on p-Polyaniline/n-TiO<sub>2</sub> Heterojunction. *Sens. Actuators B Chem.* **2008**, *134*, 988–992. [[CrossRef](#)]
169. Parveen, A.; Koppalkar, A.; Roy, A.S. Liquefied Petroleum Gas Sensing of Polyaniline–Titanium Dioxide Nanocomposites. *Sens. Lett.* **2013**, *11*, 242–248. [[CrossRef](#)]
170. Zheng, J.; Li, G.; Ma, X.; Wang, Y.; Wu, G.; Cheng, Y. Polyaniline–TiO<sub>2</sub> Nano-Composite-Based Trimethylamine QCM Sensor and Its Thermal Behavior Studies. *Sens. Actuators B Chem.* **2008**, *133*, 374–380. [[CrossRef](#)]